Photoconductive analysis of defect density of hydrogenated amorphous silicon during room-temperature plasma posthydrogenation, light soaking, and thermal annealing

J. P. Conde, M. Gonçalves, P. Brogueira, and V. Schotten
Department of Physics, Instituto Superior Técnico, Avenida Rovisco Pais, 1096 Lisbon, Portugal

V. Chu
INESC, Instituto de Engenharia de Sistemas e Computadores, Rua Alves Redol 9, 1000 Lisbon, Portugal
(Received 5 October 1995)

The photoconductivity (σ_{ph}) of thin ($\leqslant$1000 Å) hydrogenated amorphous silicon films (a-Si:H) was measured as a function of time to monitor the defect density during remote inductively coupled plasma (ICP) posthydrogenation at room temperature, light soaking (performed both before and after posthydrogenation), and isothermal annealing (performed after posthydrogenation and light soaking), and fitted to a stretched exponential curve. A decrease of $\sigma_{ph}(t)$ during posthydrogenation at room temperature was observed and related to the breaking of Si-Si weak bonds by individual hydrogen atoms. Upon thermal annealing, the initial equilibrium defect density was recovered. The stretched exponential parameters β and τ of $\sigma_{ph}(t)$ were the same for the isothermal anneals performed after light soaking and after plasma posthydrogenation, indicating that the defects introduced in both cases were of similar nature. The stretched exponential parameters β and τ of $\sigma_{ph}(t)$ were also the same for the light soaking before and after plasma posthydrogenation, suggesting that posthydrogenation did not alter the susceptibility of the material to light-induced degradation. a-Si:H samples deposited by remote ICP, hot-wire, and rf glow discharge were studied. The increase of hydrogen concentration in the samples during posthydrogenation was measured by infrared spectroscopy.

I. INTRODUCTION

Optical excitation (light soaking) and carrier injection create Si dangling bonds in the band gap of hydrogenated amorphous silicon (a-Si:H), which act as efficient recombination centers and deep traps.[1] This metastability has adverse effects on the performance of a-Si:H devices such as solar cells and thin-film transistors. Annealing at temperatures of 150–250 °C returns the material to its equilibrium state.[2] Metastability in a-Si:H is related to the conversion of strained Si-Si bonds in the exponential band tails into dangling bonds. The motion of hydrogen atoms, which can insert themselves into weak Si-Si bonds converting them into Si-H bonds and dangling bonds, has been associated with this process.[3]

In order to study the role of hydrogen in the metastability of a-Si:H, Nickel and Jackson used posthydrogenation as a method of increasing the hydrogen concentration in the a-Si:H film while keeping a roughly fixed Si network.[4] The hydrogen concentration can also be increased by varying the deposition conditions during film growth, but this may also result in a change of the Si network.[4,5] In addition, the understanding of the improved stability of a-Si:H films observed after hydrogen plasma treatment,[6] of the effects of hydrogen plasma treatment on the properties of polycrystalline silicon,[7] and of the properties of amorphous and microcrystalline silicon films prepared using the layer-by-layer deposition technique[8,9] can also gain from posthydrogenation studies.

An *et al.* showed that as many as 2×10^{21} cm^{-3} of additional H atoms can be incorporated in Si-H bonds without increasing the deep defect density at a substrate temperature of 250 °C by alternating plasma-enhanced chemical vapor deposition growth and atomic H treatment from a hot tungsten filament.[10] In addition, Nickel and Jackson found that an increase in Si-H(D) bond density up to 3×10^{21} cm^{-3}, achieved by submitting the a-Si:H film to a deuterium microwave plasma at 350 °C, did not alter the defect density in the annealed state, the Urbach energy nor the metastable defect creation.[4] In both studies, these results were interpreted as evidence that the hydrogen enters the sample in pairs, and that each broken Si-Si bond forms two Si-H bonds with a much higher probability than the breaking of a second Si-Si bond.

Bonded hydrogen in a-Si:H was shown by NMR to be distributed in a dilute phase of spatially isolated protons and a phase of clusters of approximately six protons.[11] Zafar and Schiff proposed a model in which weak Si-Si bonds on the surface of microvoids are the unhydrogenated precursors of the clustered phase.[12,13] Since placing the first hydrogen atom in a weak bond involves breaking of the bond whereas placing a second hydrogen atom does not, the first hydrogen attached is postulated in their model to be more weakly bound than the second. This model, in which these weak Si-Si bonds preferentially bind hydrogen in pairs, is analogous to a negative-U model for electronic defects (where U is the correlation energy).[14]

In both the experiments of Nickel and Jackson[4] and An *et al.*,[10] the posthydrogenation treatment was performed at temperatures above the equilibration temperature of a-Si:H. This results in simultaneous thermal annealing and posthydrogenation. In this paper, posthydrogenation is performed on a-Si:H films with thicknesses below 1000 Å *at room temperature*. In this case, an increase in the defect density of the a-Si:H upon hydrogen incorporation is found that can be fully annealed above 130 °C. The kinetics of the annealing of

TABLE I. Sample properties and deposition conditions. d: Sample thickness; E_{Tauc}=Tauc's bandgap; B_{Tauc}: B factor of Tauc's gap; σ_d: dark conductivity at 298 K; E_{act}: activation energy of σ_d in the range 0–100 °C; σ_{ph}: photoconductivity at generation rate $G=10^{21}$ cm^{-3} s^{-1} (uniformly absorbed light); γ: exponent of conductivity ($\sigma_{\text{ph}} \propto G^{\gamma}$); sccm: cubic centimeter per minute at STP.

Sample	d (μm)	E_{Tauc} (eV)	B_{Tauc} (cm eV)$^{-1/2}$	σ_d (Ω cm)$^{-1}$	E_{act} (eV)	σ_{ph} (Ω cm)$^{-1}$	γ		Pressure (Torr)	$T_{\text{substrate}}$ (°C)	Flux SiH_4 (sccm)	Flux H_2 (sccm)	Distance (cm)
MG18	0.10	1.79	1023	6.95×10^{-7}	0.60	9.98×10^{-3}	0.76	Remote rf power=350 W	4.3×10^{-2}	250	2	100	8.5
MG19	0.20	1.74	744	2.36×10^{-6}	0.50	9.50×10^{-3}	0.64	Remote rf power=300 W	4.2×10^{-2}	250	2	100	9.0
MG20	0.047	2.36	1366	3.69×10^{-11}	0.70	4.48×10^{-7}	0.93	Remote rf power=200 W	4.3×10^{-2}	250	6	94	9.0
MG22	0.08	2.13	930	2.76×10^{-9}	0.75	4.02×10^{-5}	0.66	Remote rf power=150 W	4.7×10^{-2}	250	6	92	12
IS175	0.10	1.70	684	3.38×10^{-10}	0.85	6.26×10^{-5}	0.78	Hot wire T_{filament}=1200 °C	8×10^{-1}	220	20	20	3
S366	0.08	1.69	969	3.85×10^{-10}	0.96	6.37×10^{-6}	0.61	rf power=10 W	1×10^{-1}	200	10	0	3

defects created by posthydrogenation and light soaking are compared, as well as the kinetics of light soaking before and after the sample was submitted to posthydrogenation.

II. EXPERIMENT

A. Sample preparation and characterization

a-Si:H samples prepared using three different chemical vapor deposition (CVD) techniques were studied: standard rf glow discharge, hot-filament (HFCVD) and remote inductively coupled rf glow discharge (ICP). Table I indicates typical deposition conditions and typical optical and electronic properties of the samples used in this study. In HFCVD four 16-cm-long, 0.25-mm-diam tungsten wire filaments were used. In ICP, the hydrogen was introduced in a ceramic discharge chamber surrounded by the inductive coils, while the silane was introduced through a showerhead in the main deposition chamber. In Table I, the distance indicated for ICP corresponds to the distance between the inductive discharge chamber and the substrate (this distance was also kept during the hydrogen plasma treatment), while in HFCVD it corresponds to the distance between the filament and the substrate and in rf glow discharge to the distance between the powered electrode (cathode) and the grounded substrate electrode (anode). a-Si:H samples prepared with different deposition techniques were used to verify if the observed effects of posthydrogenation depended on preparation technique.

The sample characterization shown in Table I was performed *ex situ*. MG20, MG22, IS175, and S366 show values of dark conductivity, σ_d, activation energy, E_{act}, and photoconductivity, σ_{ph}, typical of a-Si:H samples. The higher σ_d and lower E_{act} of MG18 and MG19 indicate the onset of microcrystallization (although the grain size was too small to be easily seen using Raman spectroscopy or x-ray diffraction). Each sample was subjected to a series of annealing, light-soaking, and plasma degradation treatments performed in vacuum, which are described in the next section. During these treatments, σ_{ph} was monitored in vacuum as a function of time. In general, the $\sigma_{\text{ph}}(t)$ curves fit well to a stretched exponential curve:[15] $\sigma_{\text{ph}}(t)^{-1}=\sigma_{\text{ph}}(\infty)^{-1}-[\sigma_{\text{ph}}(\infty)^{-1}-\sigma_{\text{ph}}(0)^{-1}]\exp[-(t/\tau)^{\beta}]$. τ and β were extracted[16] from a linear regression of $\ln\ln[\sigma_{\text{ph}}(t)^{-1}-\sigma_{\text{ph}}(\infty)^{-1}]/[\sigma_{\text{ph}}(0)^{-1}-\sigma_{\text{ph}}(\infty)^{-1}]$ vs $\ln t$. White light from a tungsten-halogen lamp was used with a generation rate G, of approximately 10^{19} cm^{-3} s^{-1}. σ_{ph} is proportional to $(N_r)^{-1}$ and $(N_{dd})^{-1/\gamma}$, where N_r is the number of recombination centers, N_{dd} is the number of deep defects, and the γ factor is the dependence of σ_{ph} on G ($\sigma_{\text{ph}} \propto G^{\gamma}$).[17] Hence measuring σ_{ph} is a convenient way of following the evolution of the deep defect density in a-Si:H.

B. Experimental sequence

Each sample was submitted sequentially to a series of postdeposition treatments: (i) after deposition, the sample was annealed for 1 d at 170 °C (the purpose of this annealing was to ensure the removal of deposition-induced metastable defects, and also to provide a comparable starting point, since in some samples more than one sequence of postdeposition treatments was performed); (ii) the sample was then light soaked (this was to assess its susceptibility to light-induced degradation in the annealed state); (iii) the sample was subsequently annealed in order to study the kinetics of the removal of light-induced defects; (iv) the next step was the exposure of the sample to a hydrogen ICP plasma; (v) this was followed by an isothermal anneal in order to study the kinetics of the removal of the hydrogen-plasma-created defects; (vi) a second light soaking was performed to assess if the exposure to the hydrogen plasma had any consequences in the susceptibility of the sample to light-induced degradation; (vii) finally, an isothermal anneal was performed to study the kinetics of the removal of the light-induced defects after the sample had been submitted to a hydrogen plasma. Figure 1 illustrates typical values of $\sigma_{\text{ph}}(t)$ for the experimental sequence described above. For the samples MG18, MG19, and MG20, the experimental sequence described above was performed both immediately after deposition without breaking vacuum and after exposure to the atmosphere. No difference was found between the two conditions.

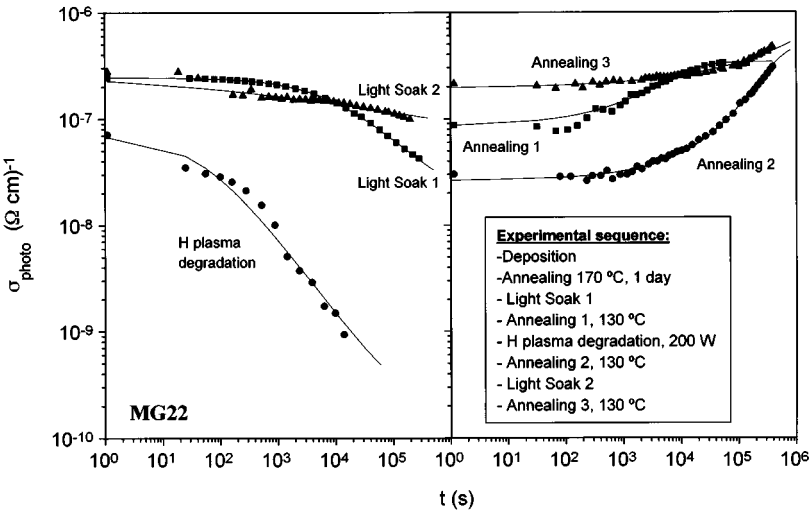

FIG. 1. Steady-state photoconductivity ($G \approx 10^{19}$ cm^{-3} s^{-1}) of a-Si:H as a function of time. The experimental sequence followed for this sample (MG22) is indicated in the inset. The lines are fits to a stretched exponential curve. σ_{ph} was measured at the annealing temperature during the annealing cycles and at room-temperature during light soaking and posthydrogenation. The discontinuities between the values of the degraded σ_{ph} and those of σ_{ph} at short annealing times are due to the annealing that occurred during the time it took to heat the sample from room temperature to the annealing temperature.

III. RESULTS

Table II shows the average values of the stretched exponential parameters β and τ for the fits of $\sigma_{ph}(t)$ for all samples. Also indicated is the number of experiments from which the average β and τ were derived. Light soaking shows a $\beta \approx 1$, both before and after plasma posthydrogenation. The characteristic time τ (which depends both on the mechanism of defect creation, and on the light intensity used) is also the same for light soaking before and after plasma degradation. Hydrogen plasma degradation occurs with a smaller average value of β (≈ 0.85) than light-soaking degradation, but the values overlap if the error bars are taken into account. Since τ is dependent both on mechanism and on power, it cannot be directly used to compare different defect-creating processes. Annealing of the light-induced defects and the plasma-induced defects occur with comparable values of β and τ (respectively ≈ 0.5 and 10^3 s). This is an indication that the defects created by light soaking and exposure to a hydrogen plasma are of the same nature.

One experimental concern was that the light emission from the hydrogen plasma could be responsible for the decrease in σ_{ph} observed during posthydrogenation. In order to verify if this was the case, the sample was exposed to the hydrogen plasma while protected by either a quartz or a glass cup that isolated the sample from the plasma, but not from the radiation. In both cases, only a slight light-soaking effect (corresponding to $G \leqslant 10^{18}$ cm^{-3} s^{-1}) was observed. This effect was clearly distinguishable from that of the hydrogen plasma exposure, since Table II shows that the characteristic time for σ_{ph} degradation by posthydrogenation is about one order of magnitude faster than that for light soaking at $G \approx 10^{19}$ cm^{-3} s^{-1}. It is thus possible to conclude that the observed decrease in σ_{ph} when the film is exposed to a remote inductively coupled hydrogen plasma is not light induced.

TABLE II. Stretched exponential parameters of photoconductivity.

Experiment	N	$\beta \pm \sigma_\beta$	$\ln \tau \pm \sigma_{\log \tau}$	$\langle \tau \rangle$ (s)
Light soak	13	1.02±0.23	5.43±0.44	2.72×10^5
Plasma degradation	19	0.85±0.20	4.17±0.87	1.48×10^4
Annealing after light soak	13	0.46±0.16	3.67±0.86	4.64 ± 10^3
Annealing after plasma degradation	10	0.52±0.15	3.27±0.92	1.87 ± 10^3
Light soak before any plasma degradation	5	1.09±0.30	5.65±0.47	4.52 ± 10^5
Light soak after first plasma degradation	8	0.93±0.18	5.33±0.38	2.16 ± 10^5

The incorporation of hydrogen during exposure to the plasma was studied using infrared spectroscopy. Table III shows the integrated infrared absorption of the Si-H bending centered around 670 cm^{-1} which is proportional to the total hydrogen content in the sample.[18–20] Although these numbers carry significant uncertainty due to the thinness of the samples, it is possible to conclude from Table III that exposure to the ICP hydrogen plasma increases the sample hydrogen content.

It has been a concern in previous posthydrogenation studies that the shallow-trap dominated diffusion coefficient should be high enough to ensure a relatively uniform H penetration throughout the film.[4,8,10] Diffusion coefficients $\geqslant 2\times10^{-15}$ cm^{-2} s^{-1} at 250 °C have been measured under conditions of posthydrogenation.[4,8,10] These values are significantly higher than those for thermal diffusion of H in undoped a-Si:H ($\approx 10^{-17}$ cm^2 s^{-1}) at the same temperature.[21] A strong reduction of the diffusion coefficient for posthydrogenation experiments performed at room temperature is expected due to the activation energy factor,[4,22] but the formation of a hydrogenated layer on the surface of the sample is

TABLE III. Infrared integrated absorption (Si-H bending).

Sample	Area before H plasma	Area after H plasma	% increase
MG22 (remote rf)	174	846	386
IS175 (hot wire)	608	730	20
S366 (rf)	971	1298	34

still expected due to hydrogen impact and diffusion by very shallow traps.[22] The hydrogenation of the sample is confirmed by the infrared measurements and is probably confined to a shallow layer on the sample surface. As long as the diffusion length of the carriers ($\approx$1000 Å in a-Si:H) is comparable to the thickness of the sample, the photogenerated carriers will probe any deep defects induced by room-temperature posthydrogenation, which will thus control the value of $\sigma_{\rm ph}$. The same sequence of light soaking, annealing, and posthydrogenation described above has also been performed on thicker samples ($\geq$2000 Å). In this case, plasma posthydrogenation caused negligible degradation in $\sigma_{\rm ph}$ and the main contribution to the degradation of $\sigma_{\rm ph}$ came from light soaking.

IV. DISCUSSION

When hydrogen is introduced in a-Si:H the most energetically favorable bonds for it to break are the $\approx 10^{20}$ cm^{-3} weak Si-Si bonds.[4] An increase in the hydrogen concentration in the sample will tend to increase the hydrogen chemical potential, $\mu_{\rm H}$. This favors the following reaction of the weak Si-Si bonds near or below $\mu_{\rm H}$:[23]

$$\mathrm{H}+(\mathrm{Si\text{-}Si})_{\rm weak}\rightarrow \mathrm{Si\text{-}H}+\mathrm{D}-. \qquad (1)$$

H corresponds to the energetic atomic hydrogen supplied by the plasma. This reaction creates a strong Si-H bond and an isolated dangling bond (D–). When the posthydrogenation is performed at room temperature, the dangling bonds created in reaction (1) are frozen-in. This results in an increase of the density of deep defects upon exposure to the posthydrogenation plasma that is responsible for the drop in photoconductivity observed (Fig. 1 and Table II). The stretched exponential behavior results from the distribution of weak-bond energies available for hydrogenation.

Upon thermal annealing, the dangling bonds become mobile and are able to diffuse, for example, from site A to site B, through a mechanism of bond switching indicated in reaction (2):[24]

$$(\mathrm{D}-)_A+(\mathrm{Si\text{-}H})_B\rightarrow(\mathrm{Si\text{-}H})_A+(\mathrm{D}-)_B. \qquad (2)$$

Eventually, two dangling bonds may meet and reform a weak bond. A possible mechanism for this to occur is indicated in reaction (3):

$$\mathrm{Si\text{-}H}-\mathrm{D}+\mathrm{D}-\rightarrow \mathrm{Si\text{-}H}+(\mathrm{Si}+\mathrm{Si})_{\rm weak}. \qquad (3)$$

The intimate Si-H–D complex is expected to occur frequently in a-Si:H. Reaction (3) is the inverse reaction to that which is often encountered in the literature as the equation that describes the microscopic mechanism for light-induced degradation.[25,26] The observation (Table II) that the annealing of light-induced defects and posthydrogenation-induced defects show the same kinetics strongly suggests that the two processes share the same underlying microscopic mechanism.

One difficulty with the simple picture described above is that since, upon incorporation of H, $\mu_{\rm H}$ is expected to increase, the Si-H concentration should increase at the expense of the weak Si-Si bond concentration, thus allowing the amorphous network to relax.[27–29] As a consequence, a sharpening of the Urbach tail is expected and, if the sample is equilibrated by annealing above the defect freeze-in temperature, a lower defect density would also be expected. However, upon posthydrogenation at 350 °C (Refs. 1 and 28) or after consecutive posthydrogenation and annealing (this work) a reduction of the deep defect density (or, equivalently, an increase in $\sigma_{\rm ph}$) was not observed. To explain this observation, it was suggested that the additional H atoms are accommodated in pairs (or in clusters), which requires that each broken Si-Si bond forms two Si-H bonds with a very high probability.[4,10,12,13] These negative-U configurations are expected, if the H concentration in these paired configurations is high enough, to pin the hydrogen chemical potential and freeze the number of deep defects, in good agreement with the experimental results. In this case, instead of reaction (3) for the annealing of the deep defects, reaction (4) would be more likely:

$$2(\mathrm{Si\text{-}H}-\mathrm{D})\rightarrow 2(\mathrm{Si\text{-}H}|\mathrm{Si\text{-}H})+(\mathrm{Si\text{-}Si})_{\rm weak}. \qquad (4)$$

The (Si-H|Si-H) represents the clustered form of hydrogen. Note that reaction (4) is the inverse reaction of the reaction proposed by Zhang *et al.* for the mechanism of light-induced degradation, in which carriers, whether electrons or holes (or both) localize on the clustered hydrogen H_2* complex, causing it to dissociate.[30] According to this mechanism, once dissociated, the isolated H atoms would become trapped at strained Si-Si bonds creating spin-active midgap defects. This mechanism, like the one described by reaction (3), also strongly suggests that the states created by posthydrogenation and light-induced annealing are the same, in good agreement with the experimental results for the annealing of these defects.

The results shown in Table II also show that there is no change in the light-induced defect creation kinetics upon posthydrogenation. This result suggests that the chemical potential remains constant upon hydrogenation. A shift up of the chemical potential, with resulting rearrangement of the gap states distribution would be expected to affect the kinetics of light-induced defect creation.[13]

V. CONCLUSIONS

The results presented are in good general agreement with those of Nickel and Jackson[4] and An *et al.*,[10] in that after posthydrogenation and anneal the H concentration in the film shows a significant increase (Table III) but no change in the defect density is observed. In addition, this work shows that when posthydrogenation is performed below equilibration temperature the defect density follows a stretched exponential increase with increasing posthydrogenation time and that a subsequent annealing is necessary to achieve equilibration. The increase in defects observed during posthydrogenation suggests that atomic hydrogen is introduced in the sample not in pairs but as uncorrelated isolated atoms and the resulting defects from their interaction with the weak Si-Si bonds can be frozen-in. The proposed clustering of H in negative-U

defects can only occur after annealing of the sample upon equilibration of the structure.

Room-temperature posthydrogenation treatments can give insight into the details of hydrogen incorporation and reactivity in *a*-Si:H. In order to develop this study further, one would need a detailed characterization of hydrogen diffusion under a hydrogen plasma at temperatures below the equilibration temperature. When the sample is exposed to a hydrogen plasma, not only atomic hydrogen, but also electrons and ions impinge on the surface. These species may also be able to break weak Si-Si bonds. Hence, it would be important to understand the details of the interaction of the hydrogen plasma with the film surface.

ACKNOWLEDGMENTS

The authors would like to thank C. Vasconcelos and R. Almeida of the Department of Materials Science, IST for the use of their FTIR spectrometer. One of us (M.G.) thanks JNICT for a fellowship BJI-1929. Partial support by the Junta Nacional de Investigação Científica e Tecnológica under Grant No. PBIC/CTM/1412/92 and Programa Ciência is gratefully acknowledged.

[1] M. Stutzmann, Philos. Mag. B **56**, 63 (1987).
[2] D. L. Staebler and C. R. Wronski, J. Appl. Phys. **51**, 3262 (1980).
[3] H. Dersch, J. Stuke, and J. Beichler, Appl. Phys. Lett. **38**, 456 (1980).
[4] N. H. Nickel and W. B. Jackson, Phys. Rev. B **51**, 4872 (1995).
[5] A. H. Mahan and M. Vanacek, *Amorphous Silicon Materials and Solar Cells*, edited by B. L. Stafford, AIP Conf. Proc. No. 234 (American Institute of Physics, New York, 1991), Vol. 234, p. 195.
[6] W. A. Nevin, H. Yamagishi, and Y. Tawada, Jpn. J. Appl. Phys. **33**, 4829 (1994).
[7] N. H. Nickel, A. Yin, and S. J. Fonash, Appl. Phys. Lett. **65**, 3099 (1994).
[8] C. Godet, N. Layadi, and P. Roca i Cabarrocas, Appl. Phys. Lett. **66**, 3146 (1995).
[9] A. Asano, Appl. Phys. Lett. **56**, 533 (1990).
[10] I. An, Y. M. Li, C. R. Wronski, and R. W. Collins, Phys. Rev. B **48**, 4464 (1993).
[11] J. Baum, K. K. Gleason, A. Pines, A. N. Garroway, and J. A. Reimer, Phys. Rev. Lett. **56**, 1377 (1986).
[12] S. Zafar and E. A. Schiff, Phys. Rev. B **40**, 5235 (1989).
[13] S. Zafar and E. A. Schiff, Phys. Rev. Lett. **66**, 1493 (1991).
[14] D. Adler and E. J. Joffa, Phys. Rev. Lett. **36**, 1197 (1976).
[15] R. A. Street, in *Hydrogenated Amorphous Silicon* (Cambridge University Press, Cambridge, 1991), p. 203.
[16] M. S. Brandt and M. Stutzmann, J. Appl. Phys. **75**, 2507 (1994).
[17] S. Aljishi, Z. E. Smith, and S. Wagner, in *Amorphous Silicon and Related Materials*, edited by Hellmut Fritzsche (World Scientific, Singapore, 1988), p. 887.
[18] M. H. Brodsky, M. Cardona, and J. J. Cuomo, Phys. Rev. B **16**, 3556 (1977).
[19] H. Richter, J. Trodahl, and M. Cardona, J. Non-Cryst. Solids **59&60**, 181 (1983).
[20] G. Lucovski, R. J. Nemanich, and J. C. Knights, Phys. Rev. B **19**, 2064 (1979).
[21] D. E. Carlson and C. W. Magee, Appl. Phys. Lett. **33**, 81 (1978).
[22] W. B. Jackson and C. C. Tsai, Phys. Rev. B **45**, 6564 (1992).
[23] R. A. Street, Phys. Rev. B **44**, 10 610 (1991).
[24] R. A. Street, in *Hydrogenated Amorphous Silicon* (Cambridge University Press, Cambridge, 1991), p. 209.
[25] M. Stutzmann, W. B. Jackson, and C. C. Tsai, Phys. Rev. B **32**, 23 (1985).
[26] M. Stutzmann, W. B. Jackson, and C. C. Tsai, Phys. Rev. B **34**, 63 (1986).
[27] R. A. Street, Phys. Rev. B **43**, 2454 (1991).
[28] D. Das, H. Shirai, J. Hanna, and I. Shimizu, Jpn. J. Appl. Phys. **30**, L239 (1991).
[29] N. M. Johnson, C. E. Nebel, P. V. Santos, W. B. Jackson, R. A. Street, K. S. Stevens, and J. Walker, Appl. Phys. Lett. **59**, 1443 (1991).
[30] S. B. Zhang, W. B. Jackson, and D. J. Chadi, Phys. Rev. Lett. **65**, 2575 (1990).